Contribution from the Chemistry Departments, University of British Columbia, Vancouver, BC, Canada V6T 1Y6, and Simon Fraser University, Burnaby, BC, Canada V5A 1S6

NMR Studies and Structure of the [3]Ferrocenophanes $Fe(\eta^5\text{-}C_5H_4\overline{S_3})(\eta^5\text{-}C_5H_3P(S)Ph_2\text{-}1,n)$ (n = 2 or 3)

Ian R. Butler,† William R. Cullen,*† F. Geoffrey Herring,*† N. R. Jagannathan,† Frederick W. B. Einstein,*‡ and Richard Jones‡

Received April 16, 1986

The structures of the [3]ferrocenophanes $Fe(\eta^5\text{-}C_5H_4(\overline{S_3}))(\eta^5\text{-}C_5H_3P(S)Ph_2\text{-}1,n)$ (n = 3, **3a**; n = 2, **3b**) have been determined by X-ray diffraction. **3a** crystallizes in the monoclinic space group $P2_1/n$ with a = 13.545 (4) Å, b = 13.132 (5) Å, c = 11.642 (4) Å, and β = 90.05 (3)° with Z = 4. The stucture was refined to R = 0.066 by using 1208 reflections. **3b** crystallizes in the triclinic space group $P\bar{1}$, a = 8.360 (2) Å, b = 11.626 (3) Å, c = 11.725 (3) Å, α = 84.06 (2)°, β = 70.26 (2)°, γ = 73.04 (2)°, and Z = 2. The structure was refined to R = 0.037 by using 2963 reflections. Both structures have eclipsed cyclopentadienyl rings, and in each case the S_3 bridge adopts only one of the two possible half-chair conformations. In solution **3a** exists as a mixture, 60:40, of diastereomers depending on the orientation of the S_3 bridge; **3b** is predominantly one diastereomer. ^1H NMR experiments including the use of the SUPERCOSY pulse sequence allow the independent assignment of all protons in the room-temperature spectrum. A rational assignment of the conformation of the S_3 bridge relative to the protons in a particular diastereomer is made on the basis of the solid-state structures.

Introduction

During the course of some recent studies in our laboratories it became necessary to establish the site(s) of metalation following the reaction of *n*-butyllithium/tetramethylethylenediamine, BuLi/TMED, with (diphenylphosphino)ferrocene (**1**).[1] The

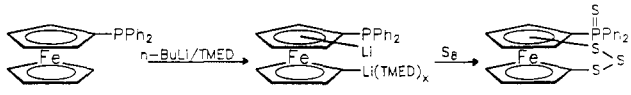

1 2 3

conventional method of derivatization with chlorotrimethylsilane gives isomer mixtures that are not easily separated. Consequently, the metalated product, principally **2**, was treated with elemental sulfur. This affords two isomers of the [3]ferrocenophane **3**, **3a** and **3b**, which can be separated by chromatography, **3a**:**3b** ≈ 3:1.[1]

There are a myriad examples of the application of 2D NMR spectroscopic methods to the solution of structural problems in organic and biological systems.[2] The adoption of this powerful technique in the realm of inorganic and organometallic chemistry has been much slower although interest is increasing as witnessed by recent communications and conference reports. For example, in one case the structures of $Re(\eta^6\text{-}C_6H_6)(\eta^5\text{-}C_7H_7)$ and $Re(\eta^6\text{-}C_6H_6)(\eta^5\text{-}C_7H_9)$ were established by a combination of 2D-*J*-resolved and 2D ^{13}C–^1H shift correlation spectroscopy.[3] In another case 2D-COSY and ^{31}P–^1H correlation experiments were used as aids in assigning the structures of an iridium(I) catalytic intermediate.[4,5]

This paper describes a series of NMR experiments that have been used to characterize the isomers of **3**. Whereas, the *J*-resolved spectroscopy was of the conventional form, the shift-correlated 2D spectroscopy employed the new pulse sequence SUPERCOSY, developed by Kumar et al.[8] This pulse scheme has considerable

Table I

formula	$FeC_{22}H_{17}PS_4$	$FeC_{22}H_{17}PS_4$
fw	496.4	496.4
cryst syst	monoclinic	triclinic
space group	$P2_1/n^a$	$P\bar{1}$
a, Å	13.545 (4)	8.360 (2)
b, Å	13.132 (5)	11.626 (3)
c, Å	11.642 (4)	11.725 (3)
α, deg		84.06 (2)
β, deg	90.05 (3)	70.26 (2)
γ, deg		73.04 (2)
V, Å^3	2070.8	1024.7
Z	4	2
D_c, g cm^{-3}	1.592	1.609
cryst dimens (max), mm	0.13 × 0.20 × 0.19	0.40 × 0.26 × 0.21
μ(Mo Kα), cm^{-1}	11.98	12.10
transmissn factors	0.776–0.882	0.743–0.809
ω_0, deg	1.30 + 0.35 (tan θ)	0.85 + 0.35 (tan θ)
ω scan speed range, deg min^{-1}	0.66–2.75	0.92–4.12
$2\theta_{max}$, deg	40	50
data collcd	$\pm h+k+l$	$+h\pm k\pm l$
cryst decay, %	7.5	±1.5
no. of unique reflcns	1921	3594
no. of obsd reflcns, $I > 3\sigma(I)$	1208	2963
no. of variables	143	258
R	0.066	0.037
R_w	0.085	0.057
goodness of fit	1.811	1.056
weighting scheme	$w = 1/(\sigma^2(F) + 0.0012F^2)$	$w = 1/(155.7t_1(X) + 205.5t_1(X) + 63.7t_3(X))$, where $X = F_o/F_{max}$[b]

[a] Nonstandard setting of $P2_1/c$, the equivalent positions are as follows: x, y, z; $^1/_2 - x, ^1/_2 + y, ^1/_2 - z$; $-x, -y, -z$; $^1/_2 + x, ^1/_2 - y, ^1/_2 + z$. [b] Weights derived from a three-term Chebyshev series.[11]

† University of British Columbia.

‡ Simon Fraser University.

(1) Butler, I. R.; Cullen, W. R. *Organometallics*, in press.
(2) (a) Kumar, A.; Wagner, G.; Ernst, R. R.; Wüthrich, K. *J. Am. Chem. Soc.* **1981**, *103*, 3654. (b) Freeman, R.; Morris, G. A. *J. Magn. Reson.* **1981**, *42*, 164. (c) Feigon, J.; Wright, J. M.; Leupin, W.; Denny, W. A.; Kearns, D. R. *J. Am. Chem. Soc.* **1982**, *104*, 5540. (d) Bhacia, N. S.; Balandrin, M. F.; Kinghorn, A. D.; Frenkiel, T. A.; Freeman, R.; Morris, G. A. *J. Am. Chem. Soc.* **1983**, *105*, 2538. (e) Rinoldi, P. L.; Salomon, R. G. *J. Org. Chem.* **1983**, *48*, 3182.
(3) Green, M. L. H.; O'Hare, D. *J. Chem. Soc., Chem. Commun.* **1985**, 333.
(4) Alcock, N. W.; Brown, J. M.; Derome, A. E.; Luey, A. R. *J. Chem. Soc., Chem. Commun.* **1985**, 575.
(5) "*J*-spectroscopy" contains chemical shift information in one frequency dimension and spin–spin coupling on the other.[6] Two-dimensional experiments of this category contain no more information than the corresponding one-dimensional experiments, but present it in a more readily interpretable form. The presence of a scalar coupling of either homo or hetero nuclei generates "cross-peaks" at the resonant frequencies of the coupled nuclei when "shift-correlated" two-dimensional spectroscopy (COSY) is employed. The observation of a cross-peak demonstrates that these nuclei are coupled to each other.[7]
(6) (a) Bodenhausen, G.; Freeman, R.; Morris, G. A.; Turner, D. L. *J. Magn. Reson.* **1978**, *31*, 75. (b) Wider, G.; Baumann, R.; Nagayama, K.; Ernst, R. R.; Wüthrich, K. *J. Magn. Reson.* **1981**, *42*, 73.
(7) (a) Bax, A.; Freeman, R.; Morris, G. A. *J. Magn. Reson.* **1981**, *42*, 164. (b) Bax, A.; Freeman, R. *J. Magn. Reson.* **1981**, *44*, 542. (c) Maudsley, A. A.; Muller, L.; Ernst, R. R. *J. Magn. Reson.* **1977**, *28*, 462. (d) Freeman, R.; Morris, G. A. *J. Chem. Soc., Chem. Commun.* **1978**, 684. (e) Morris, G. A.; Hall, L. D. *J. Am. Chem. Soc.* **1981**, *103*, 4703.
(8) Kumar, A.; Hosur, R. V.; Chandrasekhar, K. *J. Magn. Reson.* **1984**, *60*, 143.

0020-1669/86/1325-4534$01.50/0

Table II. Final Positional (Fractional, ×10⁴) and Isotropic Thermal Parameters (Å² × 10⁴) with Esd's in Parentheses for **3a**

atom	x/a	y/b	z/c	U_{eq}[a] or U_{iso}
Fe	7338 (4)	5924 (1)	5310 (2)	375
P	8584 (3)	6181 (2)	2765 (3)	395
S	9046 (3)	7552 (3)	3095 (3)	459
S(1)	6674 (3)	3520 (3)	5910 (3)	498
S(2)	6271 (3)	4242 (3)	7402 (3)	538
S(3)	5330 (3)	5378 (3)	6902 (4)	584
C(1)	7493 (9)	4398 (10)	5317 (11)	393 (36)
C(2)	7410 (9)	4775 (10)	4159 (11)	437 (37)
C(3)	8222 (8)	5474 (9)	4012 (10)	291 (32)
C(4)	8768 (10)	5503 (10)	5047 (12)	494 (40)
C(5)	8315 (9)	4833 (10)	5853 (11)	453 (38)
C(6)	6129 (10)	6269 (10)	6283 (11)	471 (39)
C(7)	6007 (10)	6611 (11)	5118 (12)	495 (39)
C(8)	6783 (10)	7321 (11)	4894 (12)	547 (41)
C(9)	7348 (10)	7371 (11)	5892 (12)	534 (40)
C(10)	6950 (11)	6737 (11)	6754 (13)	573 (43)
C(11)	7548 (8)	6131 (9)	1784 (10)	343 (34)
C(12)	7111 (10)	7037 (10)	1420 (12)	480 (38)
C(13)	6387 (12)	7025 (12)	625 (13)	659 (46)
C(14)	6038 (11)	6110 (12)	162 (13)	641 (46)
C(15)	6458 (10)	5223 (11)	528 (12)	542 (41)
C(16)	7219 (9)	5224 (10)	1331 (11)	411 (36)
C(21)	9548 (9)	5382 (9)	2136 (10)	306 (32)
C(22)	10274 (9)	5819 (10)	1461 (11)	422 (37)
C(23)	10977 (10)	5230 (10)	982 (11)	446 (37)
C(24)	11006 (10)	4212 (10)	1134 (11)	457 (38)
C(25)	10272 (10)	3745 (11)	1796 (12)	546 (42)
C(26)	9539 (9)	4335 (10)	2317 (11)	397 (36)

[a] U_{eq} is the cube root of the product of the principal axes of vibration.

potential application for larger biological molecules,[8,9] because of the reduced acqusition time to get intense cross-peaks. However, we demonstrate that it is equally applicable to other systems as well. We also report the solid-state structure of two isomers of **3** determined by X-ray diffraction methods.

Experimental Section

Compounds **3a** and **3b** were prepared according to the earlier published procedures.[1]

The NMR experiments were carried out at 400 MHz on a Bruker WH400 spectrometer at room temperature. The proton 2D-*J*-resolved, and shift-correlated experiments used the Bruker software package. For the 2D-*J*-resolved experiments, time-averaged proton free induction decays of 1024 data points were accumulated by using the standard pulse sequence reported in the literature, for 128 different values of t_1. A relaxation delay of 5 s was employed, and 32 scans were accumulated for each t_1 experiment. Sine–bell apodization was employed in both dimensions before Fourier transformation.

The SUPERCOSY experiment differs from conventional COSY in that the intensities of the cross-peaks are enhanced by the introduction of two 180° pulses of the same phase with a delay $\Delta \simeq 0.3/J$ just before and after the mixing pulse. For the samples reported here a Δ value equal to 40 ms was used. The data set consisted of a 256 × 1024 matrix, and for each value of t_1, 32 free induction decays were accumulated. Sine–bell apodization was applied in both the dimensions before Fourier transformation. The pulse sequence used is shown in Figure 3A.

X-ray Crystallographic Analyses of 3a and 3b

Crystallographic and experimental data for both compounds (which grew as block-shaped orange crystals) are given in Table I. After preliminary photographic investigations, the crystals were transferred to an Enraf-Nonius CAD4-F diffractometer. Final unit cell dimensions were obtained from the setting angles of 25 accurately measured reflections by using Mo $K\alpha_1$ radiation (λ = 0.7093 Å). Data were collected with graphite-monochromated Mo $K\alpha$ radiation by using the θ–2θ scan technique at 20 °C.

The data were corrected for Lorentz–polarization and analytically for absorption effects.[10] The structures were solved by direct methods[12] and

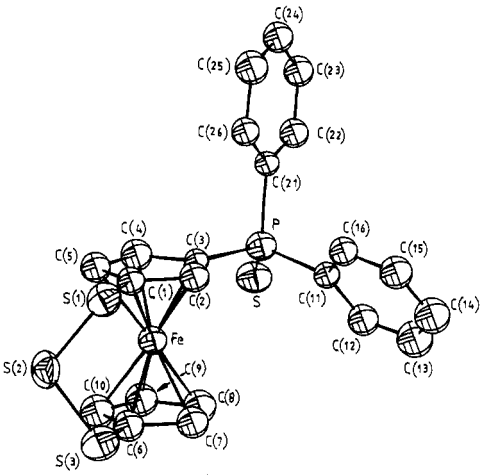

Figure 1. Structure of **3a**. The probability elipsoids are set at the 50% enclosure level.

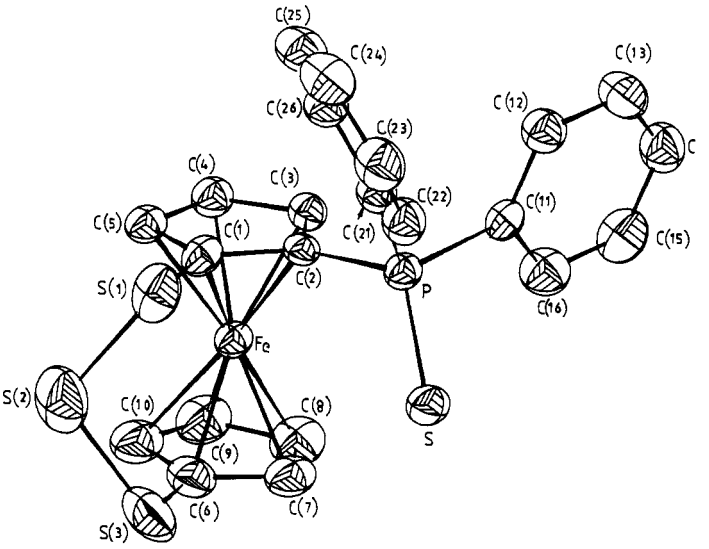

Figure 2. Structure of **3b**. The probability elipsoids are set at the 50% enclosure level.

refined by full-matrix least squares: initially with isotropic and finally with anisotropic thermal parameters (where justified). The positions of some of the hydrogen atoms were located in difference Fourier synthesis, but the positions of all hydrogen atoms were included in calculated positions (C–H 1.00 Å) and allowed to ride upon their respective carbon atoms.

Because of the limited data set in **3a**, only the Fe, P, and S atoms were allowed to vibrate anistotropically. Refinement of **3b** converged with unit weights at 0.047. However, an analysis of the variance of the reflections revealed a disturbing trend. For the $0kl$ zone, it was found that the average value of F_c/F_o was 0.87. This was attributed to potential twinning where both components of the twin overlapped for $h = 0$ but were resolved for $h \geq 1$. To account for this, a layer scale was introduced for $h = 0$. During the final stages of refinement, one reflection, which showed extinction effects, was removed. The hydrogen atoms for a given ring were assigned a common temperature factor. The final value for the layer scale, where $h = 0$, was 1.154 (5).

The highest peak in the final difference map for **3a** was 1.09 e Å^{-3} at a distance of 1.14 Å from the iron atom. The highest peak in **3b** was close to both S(1) (1.07 Å) and S(2) (1.04 Å) with a height of 0.44 e Å^{-3}.

Computations were carried out on a VAX 11/750 computer using the NRC VAX crystal structure package[13] and the CRYSTALS[14] suite of

(9) Mayor, S.; Hosur, R. V. *Magn. Reson. Chem.* **1985**, *23*, 470.
(10) Alcock, N. W. *Crystallographic Computing*; Ahmed, F., Ed.; Munksgaard: Copenhagen, 1970; p 271.
(11) Carruthers, J. R.; Watkin, D. J. *Acta Crystallogr. Sect. A: Cryst. Phys., Diffr. Theor. Gen. Chem.* **1979**, *A38*, 698.
(12) Germain, G.; Main, P.; Woolfson, M. M. *Acta Crystallogr. Sect. A: Cryst. Phys., Diffr. Theor. Gen. Chem.* **1971**, *A27*, 368.
(13) Gabe, E. J.; Larson, A. C.; Lee, F. L.; LePage, Y. *NRC VAX Crystal Structure System*; National Research Council of Canada: Ottawa, Ontario, 1984.
(14) Watkin, D. J.; Carruthers, J. R.; Betteridge, P. W. *CRYSTALS User Guide*; Chemical Crystallography Laboratory, University of Oxford: Oxford, England, 1985.

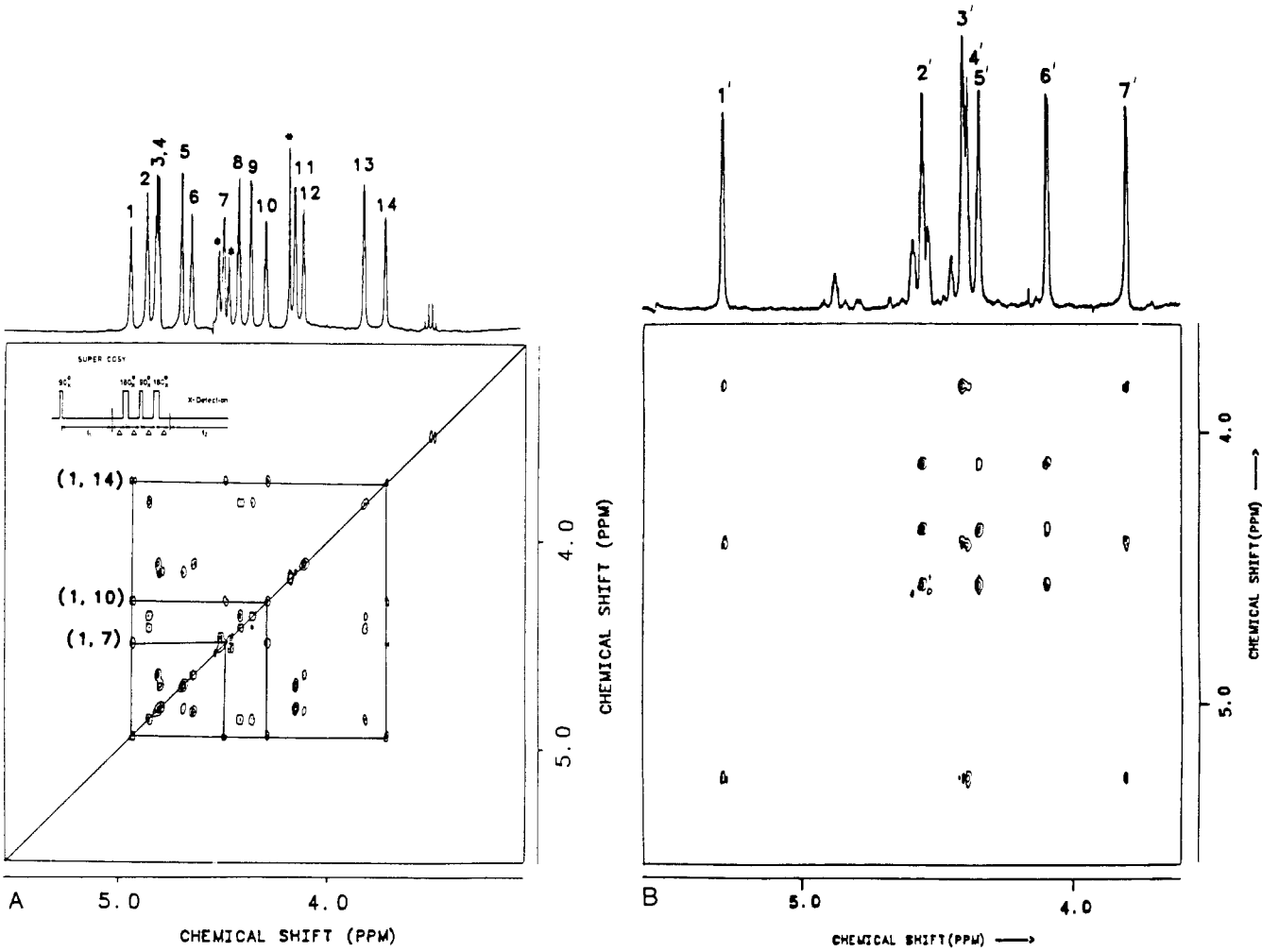

Figure 3. (A) 400-MHz SUPERCOSY contour plot of the cyclopentadienyl region of the proton NMR spectrum of **3a** at room temperature. $W1$ = 1000 Hz, $W2$ = 1000 Hz; $X1$ = 128; $X2$ = 1024; $N1$ = 256; $N2$ = 1024. Sine-bell apodization was applied in both dimensions before Fourier transformation (FT). The conventional 1D spectrum is also shown above the contour plot for convenience. Peaks marked with an asterisk are due to $P(S)Fc(Ph)_2$. (B) SUPERCOSY contour plot of the cyclopentadienyl region of the proton NMR spectrum of **3b** at 400 MHz obtained at room temperature. $W1$ = 800 Hz; $W2$ = 800 Hz; $X1$ = 128; $X2$ = 1024; $N1$ = 256; $N2$ = 1024. Sine-bell apodization was applied before FT in both dimensions. The normal 1D spectrum is shown on the top of the contour plot for convenience.

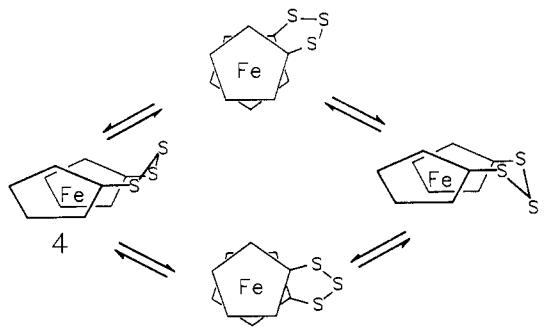

Figure 4. Fluxional behavior of the [3]ferrocenophane **4**. Adapted from ref 22a.

programs. Complex neutral-atom scattering factors were taken from ref 15. Final positional and isotropic (or equivalent isotropic, $U_{eq} = (ax_1 \times ax_2 \times ax_3)^{1/3}$) thermal parameters are given in Tables II and III, respectively. Bond lengths and angles are listed in Tables IV and V, respectively. A comparison with data from related molecules is given in Table VI. Calculated hydrogen atom positions (Tables VII and VIII), anisotropic thermal parameters (Tables IX and X), data pertaining to mean plane and torsion angles (Tables XI and XII), and calculated and observed structure factors (Table XIII) are available as supplementary material. Diagrams of **3a** and **3b** are given in Figures 1 and 2, respectively.

Results and Discussion

On the basis of the known eclipsed structure of the simple S_3-bridged ferrocenophane **4**[17] and the preferred sites of metalation of ferrocene derivatives,[1,18-20] the most likely structures of **3a** and **3b** are as shown, with **3a** being the isomers formed in greater

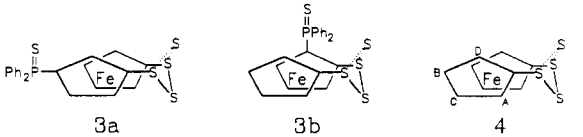

quantity. As described below, this is confirmed by their solid-state structures shown in Figures 1 and 2, although these were not known at the time the spectroscopic results were obtained.

(15) *International Tables for X-ray Crystallography*; Kynoch: Birmingham, England, 1974; Vol. 4.
(16) Davies, E. K. *SNOOPI Plot Diagram*; Chemical Crystallography Laboratory, University of Oxford: Oxford, England, 1984.
(17) Davis, B. R.; Bernal, I. *J. Cryst. Mol. Struct.* **1972**, *2*, 107.
(18) Slocum, D. W.; Engelmann, T. R.; Ernest, C.; Jones, W.; Koonsvitsky, B.; Lewis, J.; Shenkin, B. *J. Chem. Educ.* **1969**, *46*, 144.
(19) Rosenblum, M. *Chemistry of the Iron Group Metallocenes*; Wiley: New York, 1965.
(20) Slocum, D. W.; Sugarman, D. I. In *Polyamine-Chelated Alkali Metal Compounds*; Langer, A. W., Ed.; Advances in Chemistry No. 130; American Chemical Society: Washington, DC, 1974; p 222.

Table III. Final Positional (Fractional, $\times 10^4$) and Isotropic Thermal Parameters ($Å^2 \times 10^4$) with Esd's in Parentheses for **3b**

atom	x/a	y/b	z/c	U_{eq}[a]
Fe	4612.4 (8)	8508.4 (5)	2057.2 (6)	270
P	1654 (1)	6921 (1)	2067 (1)	273
S	−321 (1)	8034 (1)	3206 (1)	388
S(1)	4040 (2)	6267 (1)	4122 (1)	460
S(2)	4519 (2)	7431 (2)	5088 (1)	598
S(3)	2633 (2)	9028 (2)	5057 (1)	651
C(1)	4826 (5)	6790 (4)	2637 (4)	302
C(2)	3839 (5)	7089 (3)	1795 (4)	261
C(3)	4987 (6)	7415 (4)	678 (4)	311
C(4)	6629 (6)	7332 (4)	828 (4)	354
C(5)	6551 (6)	6945 (4)	2028 (4)	349
C(6)	3470 (7)	9546 (4)	3582 (5)	429
C(7)	2469 (7)	9923 (4)	2774 (5)	413
C(8)	3549 (7)	10270 (4)	1676 (5)	462
C(9)	5250 (7)	10104 (4)	1774 (6)	461
C(10)	5209 (7)	9664 (4)	2952 (5)	432
C(11)	1449 (5)	7057 (4)	562 (4)	287
C(12)	1632 (6)	6078 (4)	−96 (4)	401
C(13)	1422 (7)	6247 (5)	−1236 (5)	471
C(14)	1087 (7)	7383 (5)	−1741 (5)	458
C(15)	945 (7)	8362 (5)	−1105 (5)	470
C(16)	1100 (7)	8203 (4)	45 (5)	422
C(21)	1876 (6)	5353 (4)	2523 (4)	307
C(22)	441 (7)	5033 (5)	3360 (4)	387
C(23)	619 (8)	3865 (5)	3768 (5)	447
C(24)	2230 (8)	3001 (4)	3348 (4)	425
C(25)	3648 (8)	3312 (4)	2511 (5)	435
C(26)	3476 (6)	4498 (4)	2084 (4)	373

[a] U_{eq} is the cube root of the product of the principal axes of vibration.

Because the isomers contain both a disubstituted cyclopentadienyl ring (i.e. they have planar chirality) and the S_3 bridge, they can exist as diastereomers defined by the conformation of the half-chair. The ^1H NMR spectra of the isomers (omitting the $P(S)Ph_2$ region) are shown in Figure 3. In both cases 14 resonances are seen in the cyclopentadienyl region, showing that two diastereomers are present in solution. In the case of **3a** the ratio of diastereomers is 60:40 while one diastereomer predominates in the case of **3b** (>90%). The barrier to chair ⇌ chair interconversion (bridge reversal) needs to be reasonably high to permit the observation of diastereomers in solution at ambient temperature.

Other workers[21,22] have studied the bridge reversal reaction of **4** and similar molecules with the aid of variable-temperature NMR spectroscopy and find that the barrier to this process, which presumably proceeds through skew forms as shown in Figure 4, is indeed relatively high, being ~80 kJ mol^{-1} in solution. In order to fit the spectra, Osborne and co-workers[22] found it was necessary to assign the four cyclopentadienyl resonances in the static spectrum to the ring protons in the order ACBD as indicated in **4**. The lowest frequency proton resonance was assigned to proton D on the assumption that it would experience greater shielding due to the axial lone pair of the adjacent sulfur atom. The authors noted that the assignment could be reversed without affecting the numerical results.[22]

Outlined below are the ^1H NMR experiments carried out in the present investigation to fully characterize isomers **3a** and **3b**. The initial problem was to establish that the species in solution were the isomers of **3**, then to make unequivocal assignments of the resonances to particular protons.

The first NMR experiment employed in the characterization of **3** was the recently reported SUPERCOSY technique.[8] This is particularly useful in ascertaining proton connectivities in highly coupled systems such as **3**. The resulting spectra (omitting P-

Chart I

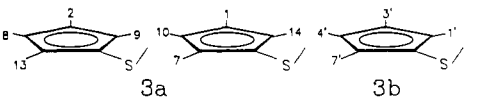

Chart II

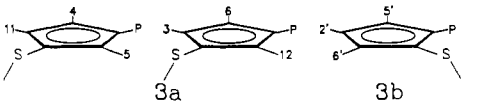

Chart III

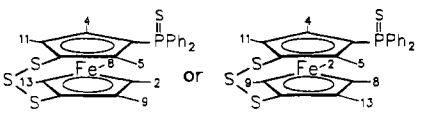

$(S)Ph_2$ regions) are shown in Figure 3. Each of the ferrocenyl proton resonances can be assigned to a particular ferrocenyl ring. Thus, for example, in Figure 3A, protons 2, 8, 9, and 13 (monosubstituted ring) and 4, 5, and 11 (disubstituted ring) arise from one diastereomer of **3a**. Similarly proton resonances 1, 7, 10, and 14 and 3, 6, and 12 arise from the other diastereomer. The situation in Figure 3B is much simplified because of the preponderance of one diastereomer of **3b**. In this case proton resonances from the monosubstituted rings are 1′, 3′, 4′, and 7′ while protons from the disubstituted ring are 2′, 5′, and 6′. Although much of this information can be obtained by application of several homonuclear proton decoupling experiments, SUPERCOSY has the advantage of yielding the desired information in one experiment. In addition where resonance overlap occurs (e.g. resonances 3 and 4, Figure 3A), making clean decoupling difficult due to bandwidth problems, this technique yields the proton connectivities easily.

The next experiment employed was homonuclear 2D-*J*-resolved spectroscopy. The spectra (ferrocenyl region only) are shown in parts A and B of Figure 5. It has been previously observed that in monosubstituted ferrocenyl rings, adjacent protons couple with a frequency of 2.5–3.0 Hz while protons separated by one carbon atom give coupling constants of ~1.2–1.6 Hz.[1,22,23] Thus typical coupling patterns for protons are shown in Figure 6. Protons adjacent to the substituent give a 1:2:2:2:1 multiplet pattern while internal protons give a 1:1:2:2:1:1 pattern. From the 2D-*J* plots, protons 1, 7, 13, and 14 in **3a** are assigned to protons adjacent to the sulfur on a monosubstituted ring while protons 1, 2, 8, and 10 are assigned to internal protons. One decoupling experiment, in each case, is sufficient to completely assign all the monosubstituted ring protons; e.g., decoupling at the well-defined resonance frequency of proton 7 results in the removal of the small coupling to proton 1, and thus protons 1 and 7 are not adjacent and consequently protons 1 and 14 are. Thus, the complete assignments to protons in the monosubstituted rings are as shown in Chart I.

To this point the identification of isomers **3a** and **3b** has not been made unequivocally by spectroscopic means. This can be done using the 2D-*J* spectrum as follows. There is a unique proton in the disubstituted ring of each isomer. In the case of **3a** the proton lies between the substituents while in the case of **3b** the proton lies between two other protons. Although both unique protons will give rise to pseudotriplets the magnitude of the couplings will be larger for **3b**. This difference is clearly seen in the 2D-*J* spectra. In Figure 5A two triplets are observed, proton resonances 5 and 12, while in Figure 5B one triplet, proton resonance 2′, is observed. The coupling constants of 2′, however, are approximately double that of the others. Therefore, **3a** and **3b** are correctly identified as drawn.

Additional information can be obtained from the residual ^{31}P–^1H couplings observed in the 2D-*J* spectra. For example, in

(21) Davison, A.; Smart, J. C. *J. Organomet. Chem.* **1979**, *174*, 321.
(22) (a) Abel, E. W.; Booth, M.; Orrell, K. G. *J. Organomet. Chem.* **1981**, *208*, 213. (b) Osborne, A. G.; Hollands, R. E.; Howard, J. A. K.; Bryan, R. F. *J. Organomet. Chem.* **1981**, *205*, 395. (c) Abel, E. W.; Booth, M.; Brown, C. A.; Orrell, K. G.; Woodford, R. L. *J. Organomet. Chem.* **1981**, *214*, 93.
(23) Maddox, M. L.; Stafford, S. L.; Kaesz, H. D. *Adv. Organomet. Chem.* **1965**, *3*, 1.

Table IV. Bond Lengths (Å) for **3a** and **3b** with Esd's in Parentheses

bond	3a	3b	bond	3a	3b
Fe–C(1)	2.015 (13)	2.020 (4)	C(3)–C(4)	1.414 (18)	1.415 (6)
Fe–C(2)	2.020 (13)	2.024 (4)	C(4)–C(5)	1.426 (18)	1.417 (7)
Fe–C(3)	2.017 (12)	2.044 (4)	C(5)–C(1)	1.398 (18)	1.430 (6)
Fe–C(4)	2.038 (13)	2.051 (4)	C(6)–C(7)	1.437 (19)	1.423 (7)
Fe–C(5)	2.050 (13)	2.045 (4)	C(7)–C(8)	1.429 (20)	1.398 (8)
Fe–C(6)	2.042 (13)	2.045 (5)	C(8)–C(9)	1.393 (20)	1.419 (7)
Fe–C(7)	2.028 (14)	2.042 (5)	C(9)–C(10)	1.412 (20)	1.415 (8)
Fe–C(8)	2.041 (15)	2.050 (5)	C(10)–C(6)	1.383 (20)	1.430 (7)
Fe–C(9)	2.018 (14)	2.041 (5)	C(11)–C(12)	1.396 (18)	1.384 (6)
Fe–C(10)	2.060 (15)	2.047 (5)	C(12)–C(13)	1.347 (21)	1.392 (7)
S(1)–C(1)	1.743 (13)	1.753 (4)	C(13)–C(14)	1.340 (22)	1.381 (7)
S(1)–S(2)	2.053 (6)	2.052 (2)	C(14)–C(15)	1.364 (21)	1.379 (8)
S(2)–S(3)	2.046 (6)	2.061 (3)	C(15)–C(16)	1.390 (19)	1.386 (6)
S(3)–C(6)	1.750 (14)	1.747 (6)	C(16)–C(11)	1.376 (17)	1.398 (6)
P–S	1.944 (5)	1.949 (2)	C(21)–C(22)	1.383 (17)	1.389 (6)
P–C(*n*)[a]	1.791 (12)	1.808 (4)	C(22)–C(23)	1.349 (19)	1.375 (7)
P–C(11)	1.810 (12)	1.817 (4)	C(23)–C(24)	1.349 (19)	1.388 (8)
P–C(21)	1.823 (12)	1.820 (4)	C(24)–C(25)	1.401 (20)	1.374 (8)
C(1)–C(2)	1.440 (18)	1.445 (6)	C(25)–C(26)	1.398 (19)	1.401 (7)
C(2)–C(3)	1.444 (17)	1.428 (6)	C(26)–C(21)	1.390 (17)	1.379 (6)

[a] For **3a** $n = 3$, and in **3b** $n = 2$.

Table V. Bond Angles (deg) with Esd's in Parentheses for **3a** and **3b**

angle	3a	3b	angle	3a	3b
S(1)–S(2)–S(3)	105.2 (3)	104.2 (1)	P–C(*n*)–C(*n*–1)[a]	129.4 (9)	126.0 (3)
C(1)–S(1)–S(2)	101.5 (5)	101.5 (2)	P–C(*n*)–C(*n* + 1)[a]	122.2 (9)	126.9 (3)
C(6)–S(3)–S(2)	102.7 (5)	102.1 (2)	S(3)–C(6)–C(7)	121.8 (10)	123.9 (4)
C(*n*)–P–S	114.1 (4)	117.1 (1)	S(3)–C(6)–C(10)	129.1 (10)	128.8 (4)
C(*n*)–P–C(11)	106.3 (5)	103.3 (2)	P–C(11)–C(12)	119.3 (9)	123.0 (3)
C(*n*)–P–C(21)	102.9 (5)	103.5 (2)	P–C(11)–C(16)	121.6 (9)	118.4 (3)
C(11)–P–S	114.0 (4)	111.9 (1)	C(12)–C(11)–C(16)	119.0 (11)	118.6 (4)
C(11)–P–C(21)	106.3 (5)	106.9 (2)	C(11)–C(12)–C(13)	120.5 (13)	120.1 (5)
C(21)–P–S	112.4 (4)	113.2 (2)	C(12)–C(13)–C(14)	121.3 (14)	120.8 (5)
C(2)–C(1)–C(5)	109.8 (11)	108.1 (4)	C(13)–C(14)–C(15)	118.2 (14)	119.7 (5)
C(1)–C(2)–C(3)	105.7 (10)	106.9 (4)	C(14)–C(15)–C(16)	121.2 (13)	119.9 (5)
C(2)–C(3)–C(4)	108.3 (11)	108.5 (4)	C(15)–C(16)–C(11)	119.9 (12)	121.0 (5)
C(3)–C(4)–C(5)	108.6 (11)	108.9 (4)	P–C(21)–C(22)	119.8 (9)	119.3 (4)
C(4)–C(5)–C(1)	107.6 (11)	107.6 (4)	P–C(21)–C(26)	120.0 (9)	120.4 (4)
C(10)–C(6)–C(7)	109.1 (12)	107.3 (5)	C(22)–C(21)–C(26)	120.2 (11)	120.2 (4)
C(6)–C(7)–C(8)	107.0 (12)	108.7 (5)	C(21)–C(22)–C(23)	120.0 (12)	120.0 (5)
C(7)–C(8)–C(9)	106.4 (12)	108.2 (5)	C(22)–C(23)–C(24)	122.3 (12)	120.4 (5)
C(8)–C(9)–C(10)	110.8 (13)	108.2 (5)	C(23)–C(24)–C(25)	119.1 (13)	119.9 (5)
C(9)–C(10)–C(6)	106.7 (13)	107.8 (5)	C(24)–C(25)–C(26)	120.0 (13)	120.2 (5)
S(1)–C(1)–C(2)	123.3 (10)	125.0 (3)	C(25)–C(26)–C(27)	118.4 (12)	119.4 (5)
S(1)–C(1)–C(5)	126.9 (10)	126.9 (3)			

[a] For **3a** $n = 3$, and in **3b** $n = 2$.

Table VI. Selected Structural Data for [3]Ferrocenophanes

	a	*b*	*c*	*d*	3a	3b
X[f]–C(1), Å	1.750 (9)	1.761 (4)	1.901 (5)	1.764 (4)	1.743 (13)	1.753 (4)
X[f]–C(2), Å	1.763 (10)	1.763 (4)	1.904 (5)	1.758 (4)	1.750 (14)	1.747 (6)
Cp mean dist, Å	1.415 (10)	1.417 (7)	1.419 (10)	1.425 (11)	1.418 (21)	1.422 (12)
Fe–C, Å	2.044 (10)	2.046 (7)	2.046 (13)	2.053 (4)	2.033 (16)	2.047 (10)
meant twist angle, deg	0.1	1.5	2.7	2.6	3.4	0.5
Cp–Cp tilt angle, deg	2.9	2.4	6.1	0.6	0.2	4.2
C(2)–C(1)–X, deg	124.3 (7)	123.5 (3)	123.9 (4)	122.8 (3)	123.3 (10)	125.0 (3)
C(5)–C(1)–X, deg	127.6 (7)	128.0 (3)	127.9 (4)	129.5 (3)	126.9 (10)	126.9 (3)
C(7)–C(6)–X, deg	123.8 (9)	123.4 (4)	123.7 (4)	122.7 (3)	121.8 (10)	123.9 (4)
C(10)–C(6)–X, deg	126.8 (8)	128.3 (4)	127.8 (4)	129.0 (3)	129.1 (10)	128.8 (4)

[a] Reference 17. [b] Reference 22b. [c] Reference 24. [d] Reference 25. [e] This work. [f] X = bridgehead atom: S for *a*, *b*, *d*, **3a**, and **3b**; Se for *c*.

Figure 5A no phosphorus coupling is observed in proton resonance 11. Such observations lead to the assignment of the disubstituted rings as shown in Chart II.

At this point each of the ferrocene molecules can be constructed from the fragments in two possible ways. For example, isomer i of **3a** can have either of the structures shown in Chart III (Chart I + Chart II).

To establish which of these possibilities is correct, a NOE difference experiment was performed in which the phenyl ortho proton resonances were irradiated. In the case of **3a** positive NOE enhancements are observed not only into proton resonances adjacent to the phosphorus substituent (4,5 and 6,12) but also into resonances 2 and 1. This implies that the phosphorus lies directly above these protons. A similar experiment conducted on **3b** showed enhancement of resonances 1′ and 5′. Thus the fully

Chart IV

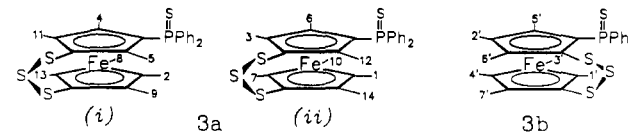

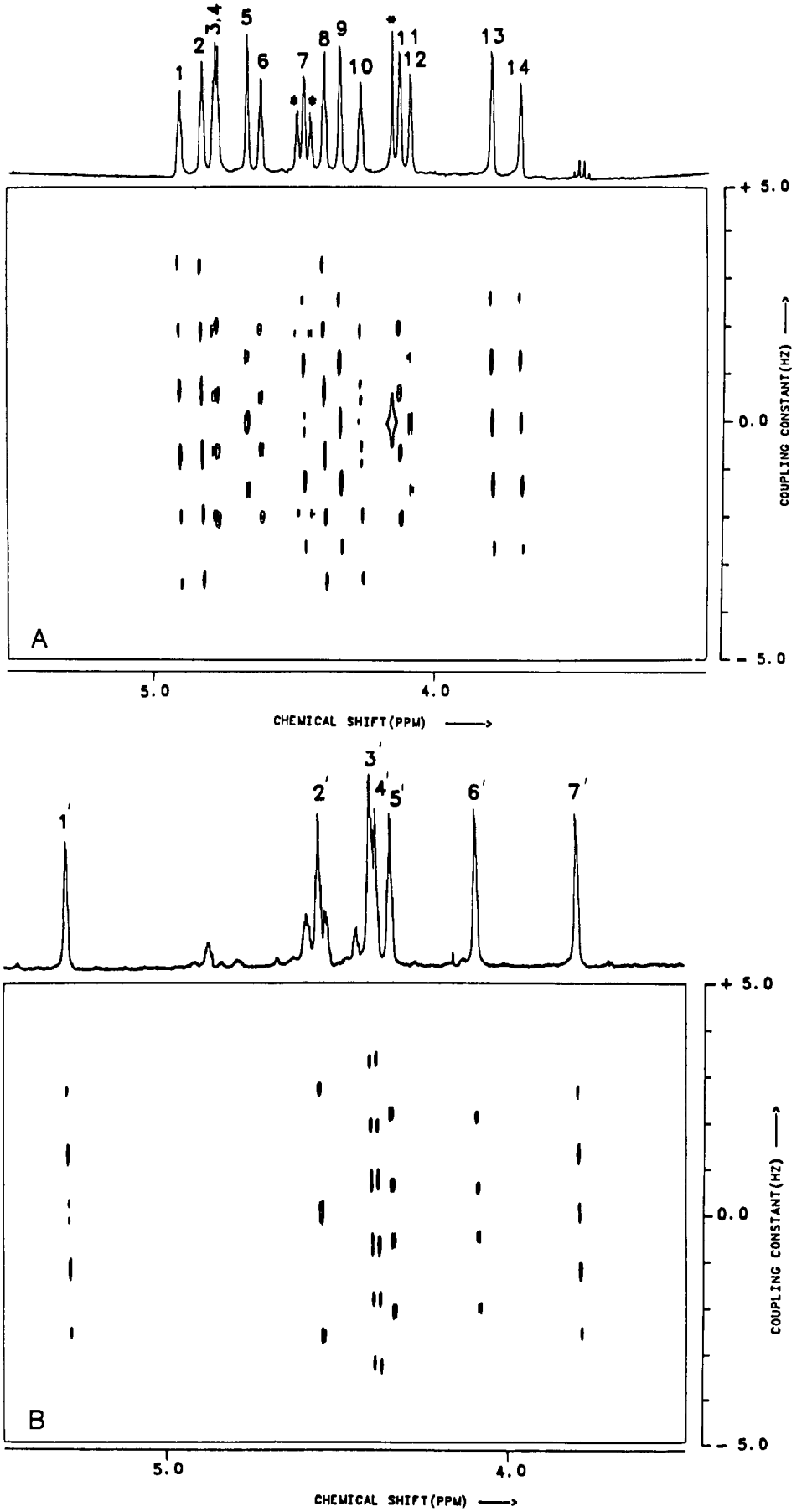

Figure 5. (A) Contour plot of the 400-MHz proton *J*-resolved 2D spectrum of the cyclopentadienyl region of **3a** at room temperature. $W1 = \pm 5$ Hz; $W2 = 1000$ Hz; $X1 = 128$; $X2 = 1024$; $N1 = 256$; $N2 = 1024$. Sine-bell apodization was applied in both dimensions before Fourier transformation. For convenience, the normal 1D spectrum is shown on the top of the contour plot. Peaks marked with an asterisk are due to $P(S)Fc(Ph)_2$. (B) Proton homonuclear 2D-*J* contour plot at 400 MHz of the cyclopentadienyl region of **3b** at room temperature. $W1 = \pm 5$ Hz; $W2 = 800$ Hz; $X1 = 128$; $X2 = 1024$; $N1 = 256$; $N2 = 1024$. Sine-bell apodization was applied in both dimensions before Fourier transformation. For convenience the 1D spectrum is shown on the top of the contour plot.

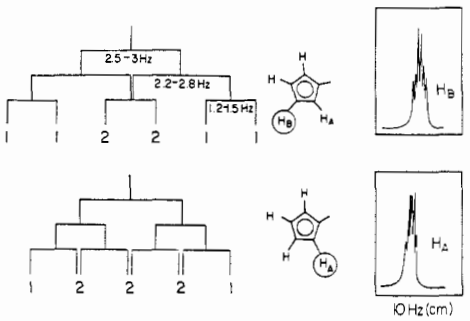

Figure 6. Stick diagrams of coupling patterns observed in a monosubstituted ferrocene ring.

assigned structures of **3a** and **3b** are shown below in Chart IV. The only uncertainty remaining lies in the orientation of the sulfur bridge, which, for the moment, should be regarded as being drawn arbitrarily.

There seems to be no unequivocal way of establishing the orientation of the sulfur rings in solution without recourse to the solid-state structures. It seems that only one diastereomer is present in the solid state for both **3a** and **3b**. Since in the case of **3b** essentially only one diastereomer is present in solution, it seems reasonable to postulate that the solution structure is the same as that of the solid. This sulfur bridge, presumably for steric reasons, is directed toward protons 7′ (and 6′), which have the two lowest resonance frequencies. Proton 1′ on the other hand has the highest resonance frequency, in fact the highest of all of the cyclopentadienyl ring protons. This seemingly well-founded conclusion is at variance with the assumptions previously made[22a] for **4** that proton D is the one which resonates at the highest frequency.

The diastereomer found in the solid state for **3a** (Figure 1) is the one indicated as isomer i in Chart IV. Since isomer i is the isomer present in greater abundance in solutions of **3a**, it is probable that the structure shown is the correct one for this isomer. On the basis of the chemical shifts noted in the previous paragraph for **3b**, the pairs of protons 11,13 and 12,14 should be found at lower frequency; 9,5 and 7,3 should be found at higher frequency. This is the case, which gives strong support for the assignments.

It should be noted that the extreme shift of proton 1′ seems to be partly due to its proximity to the $P(S)Ph_2$ group; a shift in the same direction is seen for protons 1 and 2, which have an analogous position in **3a**.

Solid-State Structures of 3a and 3b. Table VI compares selected metrical details of compounds **3a** and **3b** with those of other [3]ferrocenophanes. It can be seen that in general there is good agreement between the values observed in the present work and in previous studies, though there are slight but perceptible differences, which occur as a result of the addition of the $P(S)Ph_2$ group.

The two cyclopentadienyl rings in both **3a** and **3b** are both planar within experimental error (as are the phenyl rings) and are separated by a similar distance; viz., the average C(*n*) to C(*n* + 5) distance is 3.27 Å in **3a** and 3.29 Å in **3b**. Both molecules are almost eclipsed, with the average values of the torsion angle from a carbon atom through the centroids of the cyclopentadienyl ring to the corresponding carbon atom being 3.4 (3)° in **3a** and 0.5 (4)° in **3b**.

The angles between the ring planes are 0.2 and 4.2° for **3a** and **3b**, respectively. There are, however, marked differences in the displacements of the substituents from the cyclopentadienyl rings in the two compounds. In **3a** the sulfur bridge atoms are not significantly displaced from the plane of the rings, as is the case in **4**.[17] The phosphorus atom is displaced 0.058 Å out of the plane of the cyclopentadienyl ring, away from the center of the molecule. In compound **3b**, atom S(3) in the monosubstituted ring is again coplanar with its ring. However, in the more crowded ring, both S(1) (0.069 Å) and P (0.139 Å) are displaced from the cyclopentadienyl ring, away from the center of the molecule. The variation of the Fe–C bond lengths in **3a** shows no clear trend but

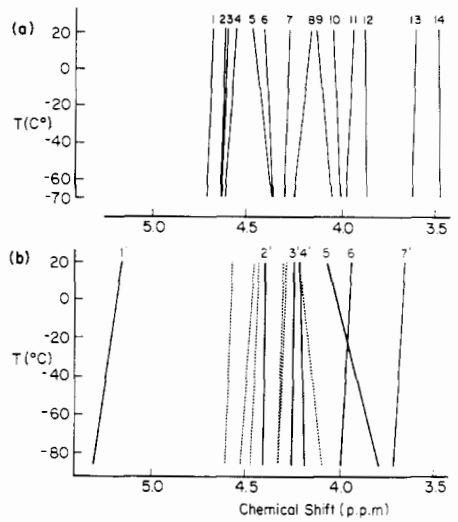

Figure 7. Effect of decreasing temperature on the proton NMR spectra of **3a** (a) and **3b** (b). The dotted lines in spectrum b represent the chemical shifts of the minor isomer of **3b**.

in **3b** those bond lengths fall into two distinct categories. The Fe–C(1) and Fe–C(2) lengths, 2.020 and 2.024 Å, respectively, are significantly shorter than the average value for all the other Fe–C bond lengths (2.046 (1) Å). The direction of the tilt of the ring in **3b** is similar to that observed in other [3]ferrocenophanes in that it minimizes the separation between C(5) and C(10).

It has been previously noted that there is a marked degree of asymmetry in the *exo*cyclic valence angle in the cyclopentadienyl ring at the bridgehead.[22,24] This has been attributed to steric interactions between C(5) and C(10) with the central atom of the bridge. The effect is clearly seen in the monosubstituted rings of **3a** and **3b** but less so in the disubstituted ring. The *exo*cyclic C–C–P bond angles in **3a** also show a marked degree of asymmetry, which is probably an attempt to relieve strain between the cyclopentadienyl ring and the $P(S)Ph_2$ group. In **3b**, the adjacent nature of the substituents reduces the tendency of the *exo*cyclic angles of either to deform, to reduce strain between the bridge and $P(S)Ph_2$ group. It would thus appear that any strain induced by the bridge and the 1,2-substitution is relieved by an increase in the tilt of the rings. This is supported by the observation that the tilt angle (4.2°) is intermediate between the value seen in **4** (2.90°)[17] and the more sterically bulky bridge in 1,3-diseleno-2,2-dichlorogermyl[3]ferrocenophane (6.1°).[25]

Other NMR Studies. As mentioned earlier the fluxional properties of [3]ferrocenophanes of this type have been the subject of considerable interest.[21,22,26] Low- and high-temperature studies on compounds **3a** and **3b** have been initiated. The high-temperature spectra of both compounds in $C_6H_5NO_2$ show similar behavior to that reported for **4** and are probably best interpreted in terms of the fluxional process shown in Figure 4. However, because of the existence of diastereomers in solution, the spectra are more complicated. These results will be reported later.

The low temperature spectra of **3a** and **3b** (CD_2Cl_2 solution) were recorded at a series of temperatures from +20 to −90 °C. The chemical shift data are shown in the form of graphs in Figure 7A,B. Examination of Figure 7A shows that proton resonances 5, 6, 9, and 10 shift to lower frequency on cooling while resonance 8 is shifted to higher frequency. In the case of compound **3b** resonances 1′ and 6′ move to higher frequency on cooling while proton resonance 5′ moves significantly to lower frequency. Similar results were found when solutions of **4** were cooled although detailed explanations are lacking.[22]

(24) Osborne, A. G.; Blake, A. J.; Hollands, R. E.; Bryan, R. F.; Lockhart, S. *J. Organomet. Chem.* **1985**, *287*, 39.
(25) Osborne, A. G.; Hollands, R. E.; Bryan, R. F.; Lockhart, R. *J. Organomet. Chem.* **1985**, *288*, 207.
(26) Butler, I. R.; Cullen, W. R.; Kim, T.-J.; Rettig, S. J.; Trotter, J. *Organometallics* **1983**, *4*, 972.

In conclusion, the present results demonstrate the applicability of 2D-NMR techniques to the elucidation of the proton NMR spectra of ferrocenophanes. Thus, once the basic data are provided by SUPERCOSY and *J*-resolved spectra, additional NOE and decoupling experiments enable the complete assignment of the proton spectra. However, in order to establish the orientation of the S_3 bridge with respect to the protons, it was necessary to use the results from solid-state structures. This combination of techniques provides, for the first time, an unequivocal assignment of the proton NMR spectrum of a ferrocenophane and should provide a basis for future studies.

Acknowledgment. The authors thank the Natural Sciences and Engineering Research Council of Canada for financial support in the form of operating grants to W.R.C., F.G.H., and F.W.B.E.

Supplementary Material Available: Tables of calculated hydrogen atom positions (Tables VII and VIII), anisotropic thermal parameters (Tables IX and X), and data pertaining to mean plane and torsion angles (Tables XI and XII) (9 pages); a table of calculated and observed structure factors (Table XIII) (40 pages). Ordering information is given on any current masthead page.

Contribution from the Department of Chemistry, Rutgers, The State University of New Jersey, New Brunswick, New Jersey 08903, and School of Chemical Sciences, University of Illinois, Urbana, Illinois 61801

Crystal Structure and Magnetic Properties of the Cluster Complex $Cu^{I}_2Cu^{II}_3[(SCH_2CH(CO_2CH_3)NHCH_2-)_2]_3\cdot 2ClO_4\cdot H_2O$, a Mixed-Valence Copper–Mercaptide Species

Parimal K. Bharadwaj,[1a] Elizabeth John,[1a] Chuan-Liang Xie,[1b] Dechun Zhang,[1c] David N. Hendrickson,*[1b] Joseph A. Potenza,*[1a] and Harvey J. Schugar*[1a]

Received June 12, 1986

The synthesis, crystal structure, electronic spectra, magnetic susceptibility (5–300 K), and EPR spectra are reported for the title complex **1**. The complex crystallizes as dark, elongated prisms in space group $P2_1$: a = 11.041 (2) Å, b = 15.820 (3) Å, c = 15.042 (3) Å, β = 98.65 (2)°, Z = 2, and R_F (R_{wF}) = 0.071 (0.073) for 3116 reflections with $I > 2\sigma(I)$. The structure contains discrete $Cu_5[(SCH_2CH(CO_2CH_3)NHCH_2-)_2]_3^{2+}$ clusters with three *cis*-$Cu^{II}N_2S_2$ units arrayed to create triangular S_3 ligation for the two Cu(I) ions. Both perchlorate anions and the water molecule are lattice species. The *cis*-$Cu^{II}N_2S_2$ units of **1** are structurally similar to the remarkably stable $Cu^{II}[(SCH_2CH(CO_2CH_3)NHCH_2-)_2]$ monomer described elsewhere. All three N_2S_2 donor sets exhibit small, similar tetrahedral distortions (18.2, 19.9, and 20.5°) as defined by the dihedral angles between the CuNS planes. Cu(II)–S distances span the range 2.237 (5)–2.266 (4) Å while Cu–N distances range from 1.965 (12) to 2.055 (11) Å. The S–Cu(II)–S, N–Cu(II)–N, and *trans*-N–Cu(II)–S bond angles span the ranges 99.8 (2)–102.2 (2), 83.2 (6)–85.7 (5), and 162.1 (3)–168.3 (4)°, respectively. Both Cu(I) ions exhibit small, comparable displacements (0.129, 0.120 Å) from their approximately triangular S_3 donor sets; Cu(I)–S distances span the range 2.232 (4)–2.291 (5) Å. The S···S contacts within the *cis*-$Cu^{II}N_2S_2$ units (3.459 (6), 3.497 (6), 3.451 (6) Å) are all slightly shorter than the van der Waals contact of 3.7 Å. Effective magnetic moments of **1** per Cu(II) fall in the range 1.74–1.79 μ_B and could be fit to the Kambe model for a triangular cluster having a small isotropic intracluster ferromagnetic exchange interaction (J = 0.26 cm^{-1}) and a TIP of -3.84×10^{-5} cgsu. At X-band frequency, the EPR spectrum of **1** (either polycrystalline or dispersed in a glycol/water glass) consists of an approximately isotropic signal at $g \approx 2.02$. Apparently, the electron-exchange coupling between the three $Cu^{II}N_2S_2$ units occurs at a frequency that exceeds the energy difference represented by the $g_\parallel$ and $g_\perp$ signals exhibited by the isolated *cis*-$Cu^{II}N_2S_2$ monomer. Electronic absorption spectra of **1** are presented and related to those observed for the isolated monomer.

Introduction

We have been interested in synthesizing models of the Cu_A site in cytochrome *c* oxidase. On the basis of published EXAFS data as well as their own detailed EPR and ENDOR studies, Chan and co-workers[2] have suggested that the Cu_A site is a pseudo-tetrahedral $CuN_2(his)S_2(cys)$ unit that has substantial Cu(II)–thiyl radical[3] as opposed to Cu(II)–thiolate character. EPR spectra of the Cu_A site are anomalous in that the g values are small (one actually falls below g = 2.00), Cu hyperfine splittings are not resolved, and the relaxation rate is large.[4] Because of the great biochemical significance of cytochrome *c* oxidase, there is considerable interest in preparing stable, paramagnetic model Cu–aliphatic dithiolates that may mimic the atypical spectroscopic signatures of the Cu_A unit. As a first approach at modeling the Cu_A unit, we have prepared a chiral *cis*-$Cu^{II}N_2(cys)S_2(cys)$ chromophore, the ligation of which is supplied by the bridged L-cysteinethiolate species $(^-SCH_2CH(CO_2CH_3)NHCH_2-)_2$.[5] The synthesis of this, as well as other, stable *cis*-$Cu^{II}N_2S_2$ chromophores proceeds without appreciable accompanying redox decomposition when macrocyclic tetramines, such as tet a, tet b, and cyclam are displaced from Cu(II) by linear tetradentate amino thiolate ligands such as the above bridged cysteine species, $(HSC(CH_3)_2CH_2NHCH_2-)_2$ or $(HSC(CH_3)_2CH_2NHCH_2-)_2CH_2$. Ligand displacement is accompanied by partial redox decomposition when $Cu(en)_2\cdot 2ClO_4$ or $Cu(H_2O)_6\cdot 2ClO_4$ are used instead of (for example) Cu(tet a)$\cdot 2ClO_4$ as starting materials. The redox decomposition product from the $Cu(en)_2\cdot 2ClO_4$ system is a mixed-valence pentanuclear complex nominally formed from the combination of 3 mol of the $Cu^{II}N_2(cys)S_2(cys)$ monomer with 2 equiv of $Cu^{I}ClO_4$. The synthesis, crystal structure, magnetic properties, EPR spectra, and preliminary electronic absorption spectra of this novel pentanuclear complex (**1**) are reported here. Other reports of mixed-valence Cu(I)/Cu(II) sulfur-bridged polynuclear species include (a) $Cu^{I}_8Cu^{II}_6[SC(CH_3)_2CH_2NH_2]_{12}Cl\cdot 3.5SO_4\cdot\approx 20H_2O$ (**2**),[6] (b) $Cu^{I}_8Cu^{II}_6[SC(CH_3)_2CH(CO_2)NH_2]_{12}Cl^{5-}$ (**3**), the D-penicillamine analogue of **2**,[7] (c) $Tl_5[Cu^{I}_8Cu^{II}_6(SC(CH_3)_2CO_2)_{12}Cl]\cdot\approx 12H_2O$ (**4**),[8] (d)

(1) (a) Rutgers University. (b) University of Illinois. (c) Visiting scholar at Rutgers on leave from Division of Chemistry, East China Engineering Institute, Nanjing, Jiangsu, China (PRC).
(2) Stevens, T. H.; Martin, C. T.; Wang, H.; Brudvig, G. W.; Scholes, C. P.; Chan, S. I. *J. Biol. Chem.* **1982**, *257*, 12106.
(3) Peisach, J.; Blumberg, W. E. *Arch. Biochem. Biophys.* **1974**, *165*, 691.
(4) Brudvig, G. W.; Blair, D. F.; Chan, S. I.; *J. Biol. Chem.* **1984**, *259*, 11001.
(5) Bharadwaj, P. K.; Potenza, J. A.; Schugar, H. J. *J. Am. Chem. Soc.* **1986**, *106*, 3151.
(6) Schugar, H. J.; Ou, C.-C.; Thich, J. A.; Potenza, J. A.; Felthouse, T. R.; Haddad, M. S.; Hendrickson, D. N.; Furey, W.; Lalancette, R. A. *Inorg. Chem.* **1980**, *19*, 543.
(7) Birker, P. J. M. W. L.; Freeman, H. C. *J. Am. Chem. Soc.* **1977**, *99*, 6890.
(8) Birker, P. J. M. W. L. *Inorg. Chem.* **1979**, *18*, 3502.

0020-1669/86/1325-4541$01.50/0